Programmable ion-sensitive transistor interfaces. II. Biomolecular sensing and manipulation

Krishna Jayant,[1,*] Kshitij Auluck,[1] Mary Funke,[2,†] Sharlin Anwar,[3,†] Joshua B. Phelps,[1] Philip H. Gordon,[1] Shantanu R. Rajwade,[1] and Edwin C. Kan[1]

[1]*School of Electrical and Computer Engineering, Cornell University, Ithaca, New York 14853, USA*

[2]*Department of Chemistry, High Point University, North Carolina 27262, USA*

[3]*Department of Biomedical Engineering, City College of New York, New York 10031, USA*

(Received 26 February 2013; revised manuscript received 8 April 2013; published 1 July 2013)

The chemoreceptive neuron metal-oxide-semiconductor transistor described in the preceding paper is further used to monitor the adsorption and interaction of DNA molecules and subsequently manipulate the adsorbed biomolecules with injected static charge. Adsorption of DNA molecules onto poly-L-lysine–coated sensing gates (SGs) modulates the floating gate (FG) potential ψ_O, which is reflected as a threshold voltage shift measured from the control gate (CG) V_{th_CG}. The asymmetric capacitive coupling between the CG and SG to the FG results in V_{th_CG} amplification. The electric field in the SG oxide E_{SG_ox} is fundamentally different when we drive the current readout with V_{CG} and V_{ref} (i.e., the potential applied to the CG and reference electrode, respectively). The V_{CG}-driven readout induces a larger E_{SG_ox}, leading to a larger V_{th_CG} shift when DNA is present. Simulation studies indicate that the counterion screening within the DNA membrane is responsible for this effect. The DNA manipulation mechanism is enabled by tunneling electrons (program) or holes (erase) onto FGs to produce repulsive or attractive forces. Programming leads to repulsion and eventual desorption of DNA, while erasing reestablishes adsorption. We further show that injected holes or electrons prior to DNA addition either aids or disrupts the immobilization process, which can be used for addressable sensor interfaces. To further substantiate DNA manipulation, we used impedance spectroscopy with a split ac-dc technique to reveal the net interface impedance before and after charge injection.

DOI: 10.1103/PhysRevE.88.012802 PACS number(s): 73.40.Mr, 82.47.Rs, 87.80.−y, 85.30.Tv

I. INTRODUCTION

Simultaneous detection and manipulation of biomolecules can open up exciting studies of the fundamental properties of proteins and DNA, controlled drug delivery, and reversible bioelectronic interfaces. While recent literature describes biomolecular detection by transistors [1–7], it has so far been very difficult to realize the opposite, i.e., using the transistor for molecular actuation. Serving as an affordable, fast, and extremely sensitive tool, the transistor platform is easier to integrate and scale than optical techniques and could also facilitate label-free readout [8]. Present nonfaradaic sensors rely on the conventional ion-sensitive field-effect transistor (ISFET) approach [7,9]. The surface of the open-gate field-effect transistor (FET) is made sensitive to ion and molecule adsorption, which subsequently modulates the transistor current. The threshold voltage in this case is measured with respect to a reference electrode, often by Ag/AgCl in a chlorine-rich buffer. However, recent efforts [5,8,10,11] have been directed towards achieving dual-gate control, which gives intrinsic amplification of the surface potential shift. Given the small size and high sensitivity of these dual-gate devices, sensing the intrinsic properties and interactions of proteins, DNA, and other small biomolecules becomes plausible [7,9].

Traditionally, the gate metal of the FET is removed and sensing is performed on the gate oxide or functional coatings. Alternatively, the gate metal can be left electrically floating and the target adsorption is on the metal surface [12]. A reference electrode such as Ag/AgCl or Pt in the electrolyte biases the transistor at the appropriate operating point. This is commonly known as the ISFET [13]. In comparison, the chemoreceptive neuron metal-oxide-semiconductor (CνMOS) [14] [Fig. 1(a)] makes use of an independently driven control gate, hence alleviating the sole reliance on the reference electrode for biasing, which can nevertheless still be used to set the bulk electrolyte potential and affect the sensor output. The use of V_{ref} can lower the read voltage to avoid read disturb, as high V_{CG} can induce unintended nonvolatile charge injection.

Optical detection schemes of DNA hybridization and protein binding rely on fluorescent labels. Not only can labeling affect the delicate nature of molecular interactions, but integrating optical detection with sub-millisecond monitoring is difficult. Chemoreceptive metal-oxide-semiconductor electrochemical sensors, in contrast, enable aggressive miniaturization, label-free operation [15], high spatial and temporal resolution, and high sensitivity based on both capacitance and charge [13,16]. Moreover, transistor detection of DNA hybridization through surface charge sensing can potentially realize electronic microassays [3,17].

Recent efforts towards dynamic control of biomolecular activity have included electrophoretic and electrochemically driven stimuli [18,19]. Electric-field manipulation is preferred compared to faradaic schemes as redox reactions often interfere and disturb the delicate molecular properties. It is also possible to ensure sufficiently high electric-field gradients with low-voltage operation [20], which is dependent on the double-layer capacitance. Under such conditions, it was proposed that the sensing electrode can still be treated as purely polarizable, as in the conventional Gouy-Chapman (GC) double-layer theory.

*Corresponding author: kj75@cornell.edu

†Contributed equally to this work.

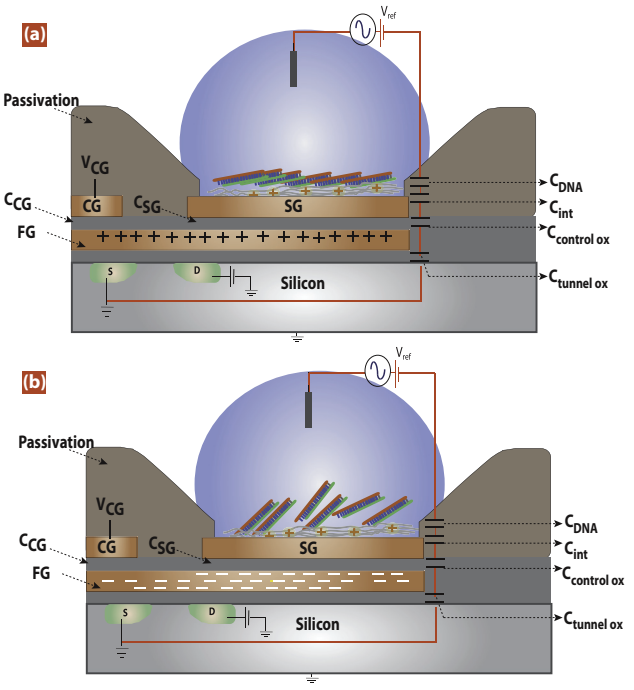

FIG. 1. (Color online) Schematic of the CνMOS transistor with independent control and sense gates: (a) DNA immobilization on the SG with FG charge erased (hole injection), resulting in DNA diffusion towards the poly-L-lysine–coated surface and (b) DNA manipulation upon programming (electron injection).

Rant *et al.* [18] provided compelling experimental evidence that the oligonucleotides' desorption occurred during an unsteady electrochemical state away from equilibrium, contrary to the notion that desorption was well captured by the GC model where an equilibrium could always be established. Similar studies by Fixe *et al.* [21] demonstrated that DNA desorption occurred after sub-millisecond pulses between a surface electrode and the bulk electrolyte, further indicating that desorption happened well before equilibrated double-layer conditions were reached. This was believed to be primarily due to counterion descreening exposing the DNA backbone, which gets electrostatically repelled, reorganizes, and then readsorbs. More recently Reddy *et al.* [22] demonstrated the effect of self-heating in silicon-on-insulator transistors as a method for local desorption with simultaneously sensing capabilities. This is an attractive alternative approach, but precise thermal control at such scales is still challenging.

In contrast, controlled nonvolatile charge injection, by either hot electron injection or Fowler-Nordheim tunneling, causes the floating gate (FG) to hold static charge of either polarity. This charge capacitively couples to the sensing gate (SG), which imparts an electrostatic force on ions (see [23]) and adsorbed biomolecules.

In this paper we present electrical monitoring of DNA hybridization and subsequent manipulation of the adsorbed biomolecules. A battery of experiments was used for calibration, including quasistatic analysis with and without the reference electrode, charge injection effects, and impedance spectroscopy through an alternative split-gate approach.

II. METHODS

A. Materials

The sensor chips were the similar to the ones used in [23]. The sensing gates were coated with poly-L-lysine (PLL) (Sigma Aldrich), set aside for 2 h and then washed with de-ionized water, dried, and stored at 4 °C before use. DNA strands B1 and B2 (see Table S-I in [24]) were procured from IDT DNA and were 99.9% high-performance liquid chromatography purified. These oligonucleotides (∼7 nm long) consisting of 20 base pairs (bp) were kept at a stock concentration of 0.5 mM in a 10 mM saline (TE) buffer (10 mM tris(hydroxymethyl)aminomethane at *p*H 8.0, 10 mM NaCl, and 1 mM ethylenediamine tetra-acetic acid). The DNA concentration used during measurements was diluted to ∼5 μM in order to achieve sufficient surface coverage without suffering from Coulombic repulsion, which normally occurs at high probe densities [25]. DNA strands (C1 and C2) (24 bp) and (D1 and D2) (48 bp) were additionally used under identical conditions to ascertain the impedance dependence on molecular length before and after hybridization. The bond pads were isolated from the sensing region via an epoxy coating, which also served as the fluid reservoir. Fluid was dispensed and removed from the well via pipettes.

B. Electrical instrumentation

In addition to the equipment used in [23] to perform IV analysis, impedance measurements were performed by monitoring the small-signal transistor gain as a function of frequency [26]. A single-toned sinusoid waveform was applied (Stanford Research Systems DS345, CA, USA) through a solution gate (Ag/AgCl reference electrode), while the dc bias was supplied via the control gate independently (Keithley 2400, USA) (see [24], Fig. S1). The output current of the transistor was fed to a lock-in amplifier (Stanford Research Systems, SR844, CA, USA) through the transimpedance amplifier (TIA). Bode responses and current-voltage IV sweeps were measured intermittently to ascertain the operating point stability. The CG was then adaptively biased to maintain a constant operating point during the impedance measurement.

III. DEVICE OPERATION AND SENSING PRINCIPLES

A. Quasistatic operations

The V_{FG} is perturbed by analyte adsorption on the SG. Upon DNA immobilization, the readout current is modulated by a change in the V_{FG} from both the SG capacitance C_{SG} and ψ_O as outlined (see [24], Table S-II). A V_{CG} sweep is then perfomed to determine V_{th_CG} when the drain current is at a constant 1 μA. As highlighted in [23], V_{th_CG}-driven readout results in an amplified measure of ψ_O and the amplification factor is primarily determined by the ratio between the two input capacitors C_{SG} and C_{CG}.

Note that DNA itself is a dielectric and hence will give rise to additional capacitive effects at the interface, which is noticable but not well understood, as the rotation angle will further affect the capactive readout [27]. The subthreshold slope is directly propotional to the total capacitance C_T (see [24], Table S-II) seen from the FG, which makes the

IV sweep a unique method to simultaneously obtain ψ_O and total capacitance. In addition, by monitoring the subthreshold slope the reliability of the device is continuously monitored since a degradation in slope can indicate ion migration into silicon for permanent device failure. In comparison, transient current measurements performed at a fixed CG bias reflects the combined effect of time-resolved shifts in ψ_O and net capacitive coupling.

B. The DNA-transistor interface

Over the past few years many models of the DNA-transistor interaction have been proposed to highlight the nature of charge modulation at the ISFET interface. Landheer *et al.* [28,29] extended the earlier study by Schasfoort *et al.* [30] and illustrated the effects of the adsorbed biomembrane as ion permeable, resulting in a Donnan potential. Kruise *et al.* [31] and McKinnon *et al.* [32] showed that high intrinsic surface charge density negated and even canceled the Donnan effect. Hence a Nernstian *p*H response is deletrious to biomolecular sensitivity. Shalev *et al.* [33], however, recently showed that the maximal sensitivity of protein detection coincided with maximal *p*H sensitivity, in direct contradiction to known theories [31]. They argued this to be due to the interaction of the protein with surface sites. This issue has still not been resolved.

The Donnan theory formulation was later improved by Liu and Dutton in [34], wherein ion permeation into the DNA layer was treated by accounting for the partition energy barrier. They explained that ion diffusion from a high-permittivity medium (bulk) to a low-permittivity medium (the DNA membrane) is always associated with an energy penalty, leading to a low ion density within the membrane. DNA orientation on the surface plays an important role as it decides the net partion energy barrier [34]. It is thus reasonable to assume that the field in the underlying oxide plays an important role in determining the overall sensitivity [32] as molecular orientation and the local ionic environment can be field dependent [35]. In this study we incorporate different ion screening profiles within and outside the DNA membrane and show that this leads to a pronounced effect on the measured ψ_O. We then present the model framework to compare different partition energy barriers for distinct configurations.

C. Impedance spectroscopy

Impedance spectroscopy was realized through small-signal analysis using a split-gate approach as CG sets the dc bias and V_{ref} delivers the ac excitation independently. This scheme has an important advantage to independently tune the transistor's dc operating point at the pixel level while maintaining a constant global ac perturbation in the buffer. DNA immobilized on the sensing gate is analogous to an additional dielectric layer with a counterion cloud, which can be modeled by an equivalent RC circuit. The main reason that justifies the RC model is that when operating at high DNA concentrations in this case ~1-5 μM, the DNA strands orient in such a way as to minimize steric interactions and reduce the overall free energy [25,36]. This results in a tightly packed film. The adsorbed DNA is also known to form an ion permeable membrane [28], which causes a fixed charge density within the adsorbed DNA film. This allows for a Donnan potential to be set within the membrane, which further affects the surface potential shifts. In the ac impedimetric mode, this introduces a strongly resistive component into the interfacial impedance in addition to the dielectric property of the DNA. The frequency responses are attributed to both resistive and capacitive changes at the interface [4,26,31]. The transfer function can be modeled by a Bode (pole-zero) plot. We point out that such impedimetric approaches can be viewed as simple two-electrode systems [6], but integrating with FETs [24,37–39] allows for simultaneous charge and capacitance estimation at the nanoscale.

The small-signal output can be represented by the simple relation [39] $v_{\text{out}} = i_d \times R_D$, where R_D is the feedback resistance and v_{out} is the small-signal output of the transimpedance amplifier. The small-signal current i_d can be approximated by $g_m v_{gs}$, where g_m is the transconductance of the amplifier and v_{gs} is the intrinsic small-signal gate-to-source voltage. The transfer function $H(j\omega)$ depicting the relaxation across the DNA monolayer accounts for the effective reduction in v_{gs}, which further relates to the output voltage by $v_{\text{out}} = g_m H(j\omega) \times v_{\text{ac}} \times R_D$. Here $H(j\omega)$ can be expanded to

$$H(j\omega) = \frac{1 + j\omega\times(R_{\text{DNA}}\times C_{\text{DNA}})}{1 + j\omega\times[R_{\text{eff}}\times(C_{\text{ox}} + C_{\text{FG bulk}} + C_{\text{DNA}})]}, \quad (1)$$

where ω and v_{ac} are the frequency and small-signal bias applied and C_{ox} is the gate oxide capacitance. The DNA monolayer is described by a resistance R_{DNA} and capacitance C_{DNA} in parallel. Here R_{eff} is the cumulative resistive contributions from the reference electrode, the electrolyte, and the adsorbed DNA film and $C_{\text{FG bulk}}$ is the parasitic capacitance from the floating gate to bulk.

The frequency response of the interfacial RC network has the pole P_1 primarily dependent on the gate oxide capacitance, associated parasitics, and electrolytic resistance. The first zero Z_1 is described by the relaxation across the DNA film at the interface. In the absence of DNA, Z_1 does not exist:

$$P_1 \cong R_{\text{eff}} \times (C_{\text{ox}} + C_{\text{FG bulk}} + C_{\text{DNA}}) \quad (2)$$

and

$$Z_1 \cong R_{\text{DNA}} \times C_{\text{DNA}}. \quad (3)$$

By performing frequency sweeps, one can monitor the properties of the adsorbed film given that the operating point is held constant. Impedance spectroscopy can also provide a suitable method to benchmark the effects of charge-injection-induced surface manipulation, as reflected in the capacitance and resistance of the interfacial layer.

IV. RESULTS AND DISCUSSION

A. Quasistatic readout

Figure 2(a) shows the variation in ψ_O upon single-stranded DNA (ssDNA) immobilization (C1) and subsequent complimentary pair addition (C2) under different biasing conditions. The SG surface is coated with PLL, which neutralizes the intrinsic hydroxyl charge, rendering it suitable for DNA adsorption. We observe that when DNA immobilization and hybridization is measured with respect to V_{ref} with V_{CG} grounded, $\Delta\psi_O$ is smaller even after compensating for

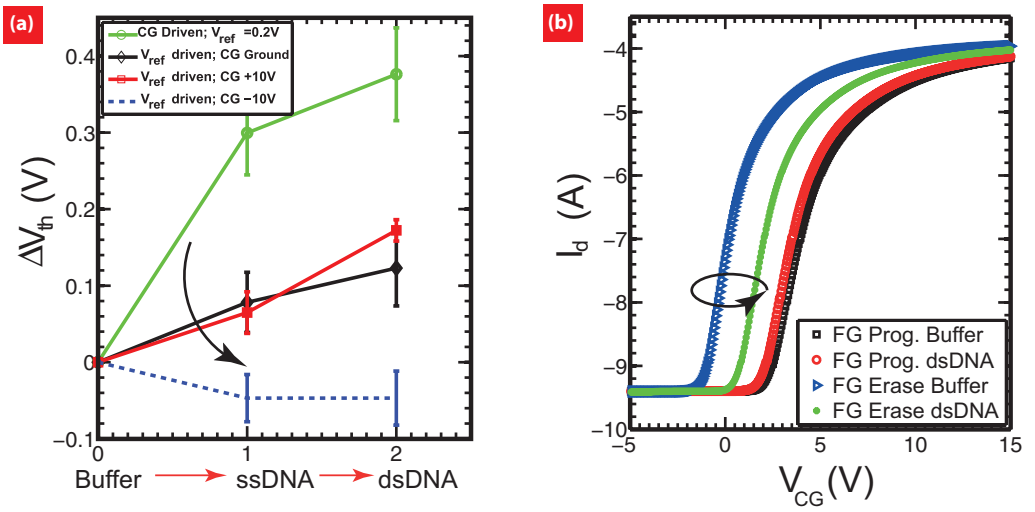

FIG. 2. (Color online) (a) Comparison between reference electrode and CG readouts during DNA immobilization and hybridization. A 10-V CG bias during V_{ref} readout renders $E_{\text{SG\_ox}}$ in the SG oxide, while a -10-V CG bias renders $-E_{\text{SG\_ox}}$. The CG-driven readout with V_{ref} at 0.2 V shows a larger ψ_{O} shift prior to hybridization mainly due to different $E_{\text{SG\_ox}}$ conditions. During hybridization, however, $\Delta\psi_{\text{O}}$ ($\sim$60 mV) is only marginally different between CG and V_{ref} readout. At $-E_{\text{SG\_ox}}$ conditions a slight reversal and diminished ψ_{O} is observed, suggesting that the underlying field affects the net charge at the interface. At such field magnitude (0.05 V/nm) DNA desorption does not occur, but the ionic screening can be perturbed. (b) Effect of electron and hole injection into the FG prior to dsDNA (24mer) addition. With electrons injected, a very small shift in $V_{\text{th\_CG}}$ is observed, which for the given capacitive ratio of $\sim$15 implies a ψ_{O} shift of approximately 10–15 mV. With hole storage the shift in ψ_{O} is $\sim$150 mV.

capacitive amplification. This is in contrast to V_{CG} readout with V_{ref} pinned at 0.2 V. We attribute this variation to differences in $E_{\text{SG\_ox}}$ during readout. A more positive $E_{\text{SG\_ox}}$ at 0.05 V/nm exists during CG readout in comparison to V_{ref} readout where $E_{\text{SG\_ox}}$ is $\sim$0.005 V/nm. This difference is balanced by a corresponding change in screening charge around the DNA molecule. The change in fields can also weakly influence the molecular orientation. We attribute this to the lower screening charge within the membrane, which results in a larger ψ_{O} shift. In order to further validate this effect, we offset V_{CG} during the V_{ref} sweep to create different $E_{\text{SG\_ox}}$ conditions. Under normal neuron metal-oxide-semiconductor operation such input offsets should only translate to a parallel shift in the transconductance responses. However, we found that under V_{CG} offsets of 10 V, $\Delta\psi_{\text{O}}$ increased slightly upon C1 and C2 addition. A positive offset resulted in larger counterion (cation) descreening within the DNA membrane. A -10-V, V_{CG} offset caused a negative $E_{\text{SG\_ox}}$ and resulted in an insensitive response. This is attributed to counterion accumulation, which screens out most of the DNA intrinsic charge. It may also affect the DNA orientation, rendering it less likely to lie flat on the surface [18,35]. We observed a much reduced shift upon ssDNA (C1) addition and very little variation upon subsequent hybridization (C2). The given V_{CG} and V_{ref} biases are too low to cause program or erase operations on the FG (see [23]). The change in $E_{\text{SG\_ox}}$ induced by a CG bias hence solely influences the DNA membrane.

In a separate study [Fig. 2(b)], in order to further corroborate field-induced DNA manipulation, we added preannealed double-stranded DNA (dsDNA) (C1 and C2) onto the SG after programming (electrons stored) and erasing charges on and off FG. In this particular example we observed $\sim$10 pC of stored charge upon programming (FG negatively charged) for a capacitive amplification factor of $\sim$15. Nominally 8–20 pC of stored charge can induce an $E_{\text{SG\_ox}} \sim \pm 0.02 - 0.2$ V/nm for the choice of capacitance ratios used in this study and also without the need for a continuously applied CG bias [23]. Such fields as described in detail in [23] can lead to shifts in ψ_{O} of $\sim$50–70 mV ($pH_B = 8$) during readout.

Once the FG is programmed or erased and DNA is added, the reference electrode and CG are temporarily floated prior to sweeping the CG bias for readout (i.e., a standby state). During this period ψ_{O} strongly tracks V_{FG}, primarily due to the strong capacitive coupling between SG and FG and weak coupling to the bulk (see [23]). We point out that the source and drain connections are not perturbed during the standby state and due to the extremely small capacitance coupling to the FG have a negligible influence on V_{FG}. Then V_{FG} is predominantly defined by Q_{FG}/C_T, which under the given conditions can reach values $\sim \pm 0.2 - 0.3$ V just prior to the readout sweep. Such dramatic changes in surface potential can strongly influence the nature of DNA immobilization and manipulation [20], as interaction with a PLL-coated surface is mainly electrostatic in nature. It is interesting to note that the ideal condition would demand a low SG-CG and a large CG-FG coupling ratio to ensure maximal field modulation by injected charge. This, however, will affect the sensitivity to analyte detection [40]. Hence it poses a design tradeoff.

In Fig. 2(b) after electron injection the shift in $V_{\text{th\_CG}}$ decreased slightly (10 mV), while a significant increase in $V_{\text{th\_CG}}$ was induced upon hole storage (–150 mV). The above experiments indicate that DNA immobilization on SGs is perturbed by attractive and repulsive force via charge-charge interaction and the underlying $E_{\text{SG\_ox}}$ can directly influence the adsorption and even the surface membrane structure. The ability to control DNA immobilization using

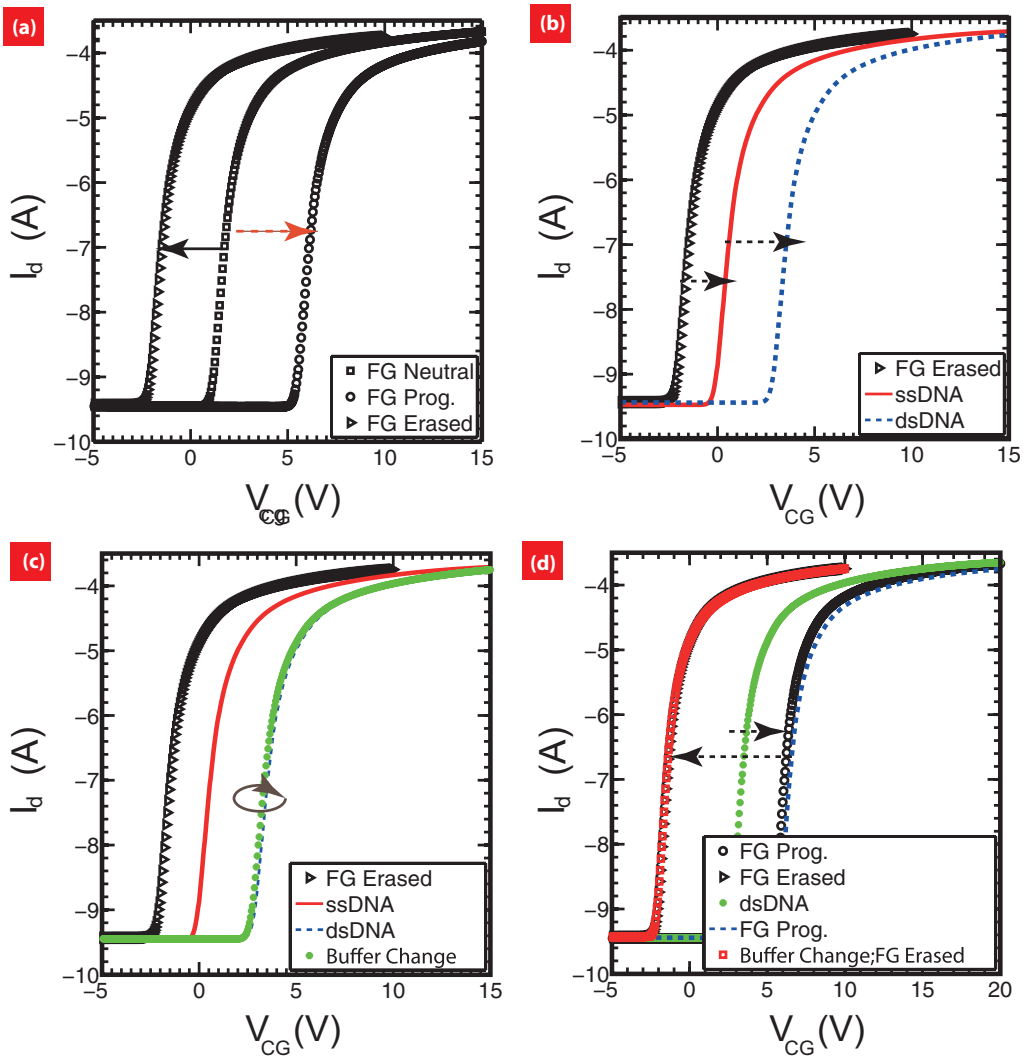

FIG. 3. (Color online) (a) The CνMOS with a poly-L-lsyine–coated sensing gate is exposed to buffer and subsequent tunneling operations are performed. The red (dashed) arrow indicates programming, while the black (solid) arrow indicates erase. (b) DNA strands C1 and C2 are added to the chip under the erased conditions (electron tunneled out), which results in marked $V_{\text{th\_CG}}$ shifts. (c) Buffer exchange after step (b) indicates an unchanged surface state. (d) Programming (electron tunneled in) the device after step (c) indicates the SG surface state is now similar to when pure buffer was present. Subsequent buffer exchange and erasing creates a refreshed interface.

programmed charge presents an opportunity to not only create addressable microarrays but also refresh the surface for continuous monitoring. For example, if hole injection promotes DNA adhesion and electron injection desorbs the adhered biomolecule, a buffer exchange after electron injection can refresh only the chosen sensor surface. We performed experiments to corroborate this hypothesis. DNA hybridization and susbequent manipulation were performed on a PLL-coated SG. A capacitiance amplification ratio of 22 was extracted prior to adding DNA. Here the reference electrode was left floating during readout to ensure maximal field modulation from the injected charge instead of the potential difference between the SG and the reference electrode. We will discuss the implications of a floating electrolyte bias in detail later. Unless otherwise mentioned, V_D was held at 1 V during IV sweeps.

Buffer was first dispensed and the IV responses were recorded during the programming and erasing cycles. A significant $V_{\text{th\_CG}}$ shift of ~8 V was observed, implying ~8 pC of stored charge [Fig. 3(a)]. Single-stranded DNA (C1) was then added under the erased condition (FG positively charged). The $V_{\text{th\_CG}}$ shift was recorded 15 min after ssDNA addition and was shown in Fig. 3(b). Repeated sweeps were performed to make sure $V_{\text{th\_CG}}$ was stable before proceeding. The arrows indicate a net $-\psi_O$ contribution at the interface. Complementary ssDNA (C2) subsequently created a further $V_{\text{th\_CG}}$ shift. We observe a $\Delta\psi_O$ on the order of ~100 mV upon C1 addition and a further 150-mV shift upon hybridization [Fig. 3(b)], consistent with previous studies on floating-gate metal-oxide-semiconductor interfaces [1,41], but in contrast to the (10–20)-mV shifts observed on conventional open-gate ISFETs [3,39,42].

Once a hybridization signal was recorded after ~40 min, we introduced a pipette filled with fresh buffer and gently sloshed back and forth 3–4 times until we replaced the entire buffer in order to remove loosely bound DNA. We observed no $V_{\text{th\_CG}}$ shift [Fig. 3(c)], which was likely due to the firmly immobilized

DNA. We then programmed (electron injection) at this stage and observed the $V_{\text{th\_CG}}$ shift. During tunneling the V_{CG} pulse was maintained for ~30 sec. If the DNA molecules were to still be immobilized to the SG after programming, we should have observed a further increase in $V_{\text{th\_CG}}$. However, we observed that the $V_{\text{th\_CG}}$ coincided with the curve corresponding to the pure buffer response with injected electrons [Fig. 3(d)]. At this point, we performed another buffer exchange to remove any loosely bound DNA as a consequence of electron injection. After a subsequent erasing operation we found that the $V_{\text{th\_CG}}$ overlapped with the trace corresponding to pure buffer as shown in Fig. 3(d). It is critical to note that throughout the experiment the subthreshold slope did not degrade, which is critical from a reliability perspective.

We also compared the effects of programming and erasing FG with and without buffer exchange (see [24], Fig. S2). The measurements indicated that after electrons were injected and subsequently erased and without replacing the buffer, $V_{\text{th\_CG}}$ recovered to the same point. Complete $V_{\text{th\_CG}}$ recovery was obtained only with electron injection and buffer exchange. This suggested that injection manipulated and weakened the DNA surface interaction, allowing complete desorption during the buffer replacement. However, without buffer exchange, DNA would be re-adsorbed.

During the initial rising CG pulse, V_{FG} increases and after 10 ms a significant amount of electrons begin to tunnel onto the FG. This electron accumulation in turn reduces V_{FG} (i.e., a negative feedback). When the CG and reference electrode are momentarily open circuited prior to readout, V_{FG} is highly negative and strongly couples to the SG, as previously mentioned. DNA is then strongly manipulated, i.e., DNA manipulation possibly occurred even before a steady-state condition (readout) was reached. This is in line with results by Rant *et al.* [18]. Figures 2 and 3 hence suggest that under $E_{\text{SG\_ox}}$ conditions, DNA is attracted towards the surface, but after FG programming the DNA desorbs as it interacts with the stored electrons. The dynamics of manipulation during and just after the tunneling operation is still actively being resolved.

B. The DNA-transistor interface model

In order to corroborate the potential shifts and understand the true nature of the observed signals, we simulated the DNA interface stack [Fig. 4(a)] using the following approach. The total charge density within the DNA membrane is given by $\rho_{\text{DNA}} + \rho_{\text{ions}}$, where ρ_{ions} is a function of ψ. The total screening charge in the DNA membrane is then given by

$$\frac{d^2\psi}{dx^2} = -\left(\frac{\rho_{\text{DNA}} + \rho_{\text{ions}}(\psi)}{\varepsilon_{\text{eff}}}\right), \tag{4}$$

where ρ_{DNA} is a constant background charge, i.e., similar to how dopants in a semiconductor are treated. Ions are mobile and are akin to electrons and holes.

We reformulate (4) into the form

$$\int_{E_{\text{O}}}^{E_{\beta 1}} E\,dE = -\frac{1}{\varepsilon_{\text{eff}}}\rho_{\text{DNA}}(\psi_\beta - \psi_{\text{O}}) - \frac{1}{\varepsilon_{\text{eff}}}\int_{\psi_{\text{O}}}^{\psi_\beta} \rho_{\text{ions}}(\psi)d\psi. \tag{5}$$

Here ε_{eff} is the effective permittivity of the DNA membrane, the subscript β represents the boundary between the DNA and bulk electrolyte presented in Fig. 4(b), and E_{O} represents the field in the DNA membrane at the oxide interface such that it satisfies the condition $\varepsilon_{\text{ox}}E_{\text{ox}} = \varepsilon_{\text{eff}}E_{\text{O}}$. A Stern layer has not been assumed in the present simulation. Similarly, the region from the DNA membrane into the bulk shown in Fig. 4(b) is reformulated as

$$\int_{E_{\beta 2}}^{0} E\,dE = -\frac{1}{\varepsilon}\int_{\psi_\beta}^{0} \rho_{\text{ions}}(\psi)d\psi, \tag{6}$$

where $\varepsilon_{\text{eff}}E_{\beta 1} = \varepsilon E_{\beta 2}$ across the DNA electrolyte interface as a discontinuity in the electric field would exist due to the differences in permittivity. Here ε is the dielectric constant of water and $E_{\beta 2}$ represents the field condition in the electrolyte across the DNA membrane. Combining Eqs. (5) and (6) we get

$$\int_{E_{\text{O}}}^{E_{\beta 1}} E\,dE + \int_{E_{\beta 2}}^{0} E\,dE = -\frac{1}{\varepsilon_{\text{eff}}}\rho_{\text{DNA}}(\psi_\beta - \psi) - \frac{1}{\varepsilon_{\text{eff}}}\int_{\psi_{\text{O}}}^{\psi_\beta} \rho_{\text{ions}}(\psi)d\psi - \frac{1}{\varepsilon}\int_{\psi_\beta}^{0} \rho_{\text{ions}}(\psi)d\psi. \tag{7}$$

In order to describe the physical mechanisms of signal generation when DNA adsorbs to the surface of the transistor we examine two approaches. In the first approach using Eq. (7) the screening models inside and outside the membrane are treated differently while permittivities are the same i.e., $\varepsilon_{\text{eff}} = \varepsilon$ throughout. We compare the Debye-Hückel (DH) formulation in Eq. (8) and the Poisson-Boltzmann (PB) formulation in Eq. (9) both inside and outside the membrane and solve Eq. (7) self-consistently in a background DNA volume charge density of ~5 C/cm^3, as shown in Fig. 4(c). In the second approach we examine the critical role of varying ε_{eff} within the PB framework inside the membrane given the same DNA volume charge density:

$$E\frac{dE}{d\psi} = -\frac{2en_{\text{O}}}{kT\varepsilon_{\text{eff}}}\left(\frac{e\psi}{kT}\right) \quad \text{(DH)}, \tag{8}$$

$$E\frac{dE}{d\psi} = -\frac{2en_{\text{O}}}{kT\varepsilon_{\text{eff}}}\sinh\left(\frac{e\psi}{kT}\right) \quad \text{(PB)}. \tag{9}$$

We begin the discussion by first considering the effect of different ion screening profiles in the DNA layer. We find that when the DH approximation is used within the membrane $\Delta\psi_{\text{O}}$ varies much more in comparison to the PB model [Fig. 4(c)]. This essentially stems from the strong nonlinear screening property imposed by the PB approximation. In principle, one could reason the use of either approximation by understanding the respective constraints. The PB model treats ions as a continuous quantity and overestimates the screening charge. If close packing of DNA does occur, which is common at μM concentrations, the volume occupied by DNA is roughly estimated to be two-thirds of the total available volume within the layer [36]. The presence of a large ion density within the membrane is thus energetically unfavorable. This necessarily implies a low ion screening within the DNA membrane, which can be mathematically treated via the DH approximation. This line of thinking is

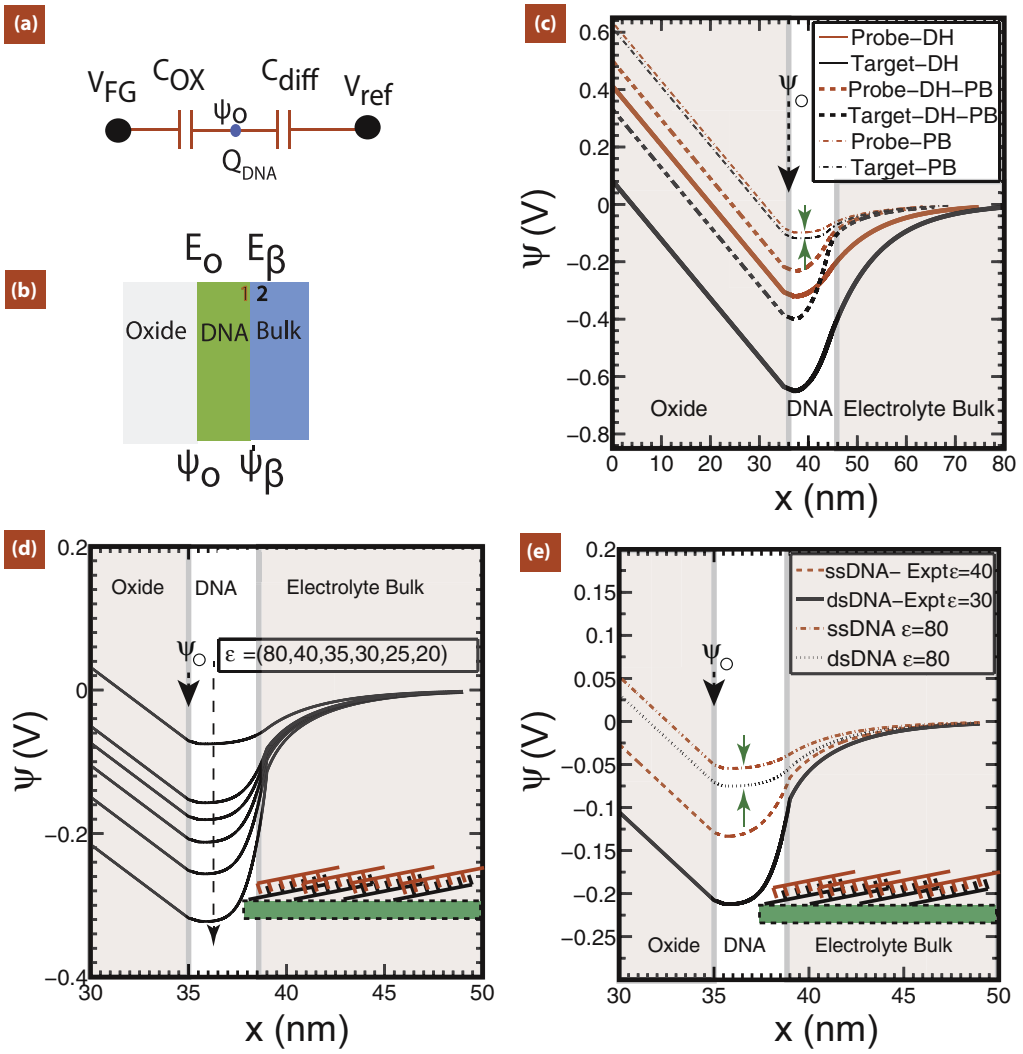

FIG. 4. (Color online) (a) Simplified capacitive model representing the FG-DNA interface. (b) DNA-SG model representing the various interfaces, potentials, and fields. Here ψ_O and ψ_β represent the potentials at the SG interface and DNA-electrolyte interface, respectively; E_O and E_β are the respective fields across the SG interface and DNA electrolyte interface, respectively; and the numbers 1 and 2 represent the discontinuity in the electric field across the DNA-electrolyte interface due to permittivity differences. (c) Potential profile across the capacitive network shown in (a) for various ionic screening models within the DNA membrane. Debye Hückel (DH) screening represents the linearized Poisson-Boltzmann (PB) approximation. Notice that when ionic screening both within and outside the membrane is low, the ψ_O shift is maximum. The nonlinear PB approximation results in a much lower shift in ψ_O. (d) Potential profile including the partition energy barrier to account for the ion charge density within the DNA membrane. The self-energy of ions ΔG_m is lowered in the DNA membrane represented by varying ε_{eff}. This leads to a lower charge density within the DNA membrane and larger change in ψ_O. The inset depicts the orientation of DNA considered in the simulation. (e) Comparison of $\Delta\psi_O$ hybridization signals between a PB approximation with $\varepsilon_{\text{eff}} = 80$ and an approximate ε_{eff} extracted for CG-driven experimental data. Experimental evidence indicates tight packing of DNA at the surface, resulting in ion exclusion and a more pronounced ψ_O shift.

similar to an inference by Wong and Melosh in [36], where they found the best agreement to experimental hybridization data to occur when counterions were completely excluded from the DNA membrane. We do point out that when DNA molecules are loosely packed and the Donnan potential fully forms, the use of the DH approximation is incorrect and the PB approximation should be employed instead. Using a DH approximation outside the membrane is theoretically incorrect, but is shown here only for intuitive purposes. Both Windbacher *et al.* [43] and Heitzinger *et al.* [44] recently proposed a linearized PB approach to tackle such screening effects similar to the DH approximation. The combination of DH inside the membrane (weak ionic screening) and PB outside (strong screening) matches closest to experiment. The use of positive electric fields can only amplify this effect [36]. Field-induced counterion descreening causes more of the DNA charge to be exposed to form a depletion zone (i.e., a region devoid of movable ions with a background DNA charge). The depletion region would increase the built-in voltage, which in this case is the Donnan potential [32]. This hypothesis strongly supports both our and previous experiments, where unexpectedly large ψ_O shifts have been observed [1,42]. Treating the charge inside the membrane using the DH model provides an intuitive understanding of how ψ_O varies when

the membrane is poorly screened, but this is a brute force method to account for ψ_O variations and raises the question as to what physical mechanism causes a lower screening.

Liu and Dutton [34] treated the ionic screening inside the DNA membrane using a partition energy ΔG_m formulation with the PB approximation. In Fig. 4(d) the potential profile is plotted for different ε_{eff} values. An energy cost is incurred when ions diffuse from the electrolyte with a higher permittivity into the DNA membrane with a lower permittivity. This partition effect primarily stems from the Born charge-dielectric interaction [34]. For the overall energy to be a minimum, a low counterion charge within the DNA membrane is required. The low ionic charge density directly translates to a lower screening within the DNA membrane. The self-energy of the ion transferred from a medium of low dielectric constant to one of high dielectric constant is treated via the relation [45]

$$\Delta G_m = -\frac{69z^2}{a}\left(\frac{1}{\varepsilon_{\text{eff}}} - \frac{1}{\varepsilon_{\text{medium}}}\right)^* 0.010\,36 \qquad (10)$$

(in eV). Here a is the ion radius and z is the valence. For $a = 1.1$ Å, $z = 1$, $\varepsilon_{\text{medium}} = 80$, and $\varepsilon_{\text{eff}} = 20$, we find $\Delta G_m = -0.243$ eV.

Ion hydration and polarization effects at the SG interface have not been considered here, but as recently discussed by Fromherz [46], such effects can further riddle the measured ψ_O. A large negative ΔG_m implies a lower ion charge density within the DNA membrane as it is energetically favorable and hence less screening. Such effects have been considered to be orientation dependent and are stronger with the strands parallel to the SG interface [32,47] and/or tightly packed [36]. This leads to a qualitatively similar result to the DH model, but is mathematically more robust. From the measurements presented in Figs. 2 and 3 for CG-driven sensing, we extracted $\varepsilon_{\text{eff}} \sim 40$ when ssDNA immobilizes ($\Delta\psi_O \sim 150$ mV) and an additional decrement to $\varepsilon_{\text{eff}} \sim 30$ when hybridization occurs ($\Delta\psi_O \sim 70$ mV) [Fig. 4(e)], assuming the strands lie parallel to the surface [Figs. 4(d) and 4(e), insets]. This is a reasonable approximation as the lysine-DNA interaction is purely electrostatic in nature. It is clear from both approaches that the net screening within the membrane severely affects the measured ψ_O. If one does not consider the drop in ε_{eff}, the difference in the hybridization signal drops down to ~20 mV, as shown in Fig. 4(e). Since a significant fraction of experimental observations in relation to DNA hybridization indicate $\Delta\psi_O$ values in the (40–120)-mV range and as such can only be justified by either weak screening or ion exclusion from the membrane, we believe that the major factor determining ion exclusion is the partition effect and the Born charge-dielectric interaction is an important source of ΔG_m. Nevertheless, a clear relation between ΔG_m and the electric field is still lacking.

C. Dual-gate operation and ψ_O amplification

We observed CG-driven (Figs. 2 and 3) ψ_O shifts of ~120−300 mV upon ssDNA addition and a further ~100-mV shift upon hybridization. Conventional Gouy-Chapman-Stern theory [3] cannot account for such large ψ_O shifts due to strong nonlinear screening. From measurements presented earlier we extract an average charge density of ~0.04 C/m^2 (immobilized ssDNA) and a subsequent ~0.02 C/m^2 during hybridization. With traditional ISFETs [3,39,42], however, DNA adsorption and hybridization normally reveal ψ_O shifts of ~40 and ~ 5−20 mV, respectively. The plausible reasons for such differences are as follows.

(i) Although influenced by the Donnan potential, ψ_O also depends on the surface pH response since a pure Nernstian response would effectively screen any membrane charge from the FG [31]. The pH response of the CνMOS is extremely non-Nernstian with and without a PLL coating and $p\text{H}_{\text{PZC}}$ was found to be closer to $p\text{H} = 9$ (not shown). The PLL coating in addition neutralizes most of the surface charge and also makes it slightly positive, resulting in a nonmonotonic and weak pH response especially around $p\text{H}_{\text{PZC}}$ (low N_S in [23]). This can enhance the Donnan effect and thereby lead to larger surface potential [29].

(ii) The Born charge dielectric function can play a significant role in amplifying the ψ_O shift.

(iii) The high surface charge of 0.8 C/m^2 normally used for SiO_2 [3] is orders of magnitude higher than the surface charge density observed in this study 8 mC/m^2 (see [23]) for polysilicon with and without PLL. Such high sheet charge densities can lead to high negative ψ_O potentials, screen out most of the DNA charge, and often interfere with DNA immobilization affecting the Donnan equilibrium and orientation.

(iv) The majority of ISFET sensors use a constant readout current when monitoring DNA binding and hybridization. This implies a constant field across the gate oxide between the two-dimensional electron-hole gas in the channel and the reference electrode. In the CνMOS due to the different $E_{\text{SG\_ox}}$ conditions when driven from the CG, ψ_O can vary by a few kT/e. This can influence DNA immobilization due to Coulombic interactions [48], resulting in counterion descreening and reorientation on the surface [18,44]. Interfacial polarization [46] can cause further modulation.

Using the circuit representation shown in Fig. 4(a), we can additionally show that the change in ψ_O differs in the three measurement conditions

$$\Delta\psi_O = \frac{\Delta Q}{C_{\text{SG}} + C_{\text{diff}}} \qquad (11)$$

when V_{ref} is grounded and the CG is driven. In contrast,

$$\Delta\psi_O = \frac{\Delta Q}{C_{\text{diff}}} \qquad (12)$$

when V_{ref} is driven and the CG is grounded. In the case when V_{ref} is floating, the change in ψ_O can be written as

$$\Delta\psi_O = \frac{\Delta Q}{C_{\text{SG}}}. \qquad (13)$$

One readily notices that the readout mechanism can severely affect the measured ψ_O. For example, CG and V_{ref} readouts are dominated by the diffusive capacitance. Equations (11) and (12) seemingly imply that V_{ref} readout would always result in a slightly higher $\Delta\psi_O$. However, $Q_{\text{DNA}} + Q_{\text{ions}}$, which makes up ΔQ, can be different under different $E_{\text{SG\_ox}}$, which can arise when V_{th} is measured from the reference electrode as opposed to CG. Hence, by appropriate sizing of

the CG and SG areas, the sensitivity to DNA detection can be maximized by engineering the ΔQ dependence on the electric field. Additionally, when V_{ref} is floating [Eq. (13)], $\Delta\psi_{\text{O}}$ can swing (∼150 mV) much more [Fig. 4(b)] in comparison to when V_{ref} is pinned (∼70 mV) (Fig. 2) primarily because the screening capacitance of the ionic diffuse layer is much lower. This suggests that the operation of the reference electrode needs more careful evaluation in order to achieve maximum sensitivity. Since the $p\text{H}_{\text{PZC}}$ lies in between $p\text{H} = 7$ and 9, when the FG is charge neutral and given evaporation was negligible during the course of experimentation, we strongly believe the enhancement in $\Delta\psi_{\text{O}}$ represented in Figs. 2 and 3 stems from the shift in Q_{ions} within the DNA membrane due to differences in $E_{\text{SG\_ox}}$.

D. Impedance spectroscopy

In order to further validate DNA desorption upon charge injection, we performed impedance spectroscopy [26,49], which probes the dielectric properties of the interface and is not dependent on surface potential and pH fluctuations [4]. This test would help ascertain whether DNA truly desorbs as monitored by the interfacial impedance change. By using the split-gate approach (Sec. II), the small-signal output is monitored through a lock-in amplifier. An important point is that the bandwidth is determined by the combined effect of the CνMOS gate stack and the parasitic FG to bulk capacitance, leading to a rolloff at approximately 300 KHz, well within the lock-in amplifier and TIA bandwidth. The overall time constant of the Bode response was reported [4,39] and also shown to be dependent on the contact-lane capacitance (∼10 nF) and electrolyte resistance, which results in the first pole at fairly low (on the order of KHz) frequencies. In the present study, however, the bandwidth of the overall response was limited by the external amplifier. The contact-lane capacitance consists of the source-drain contact line parasitics in parallel to the gate oxide capacitance. SPICE simulations with estimated parameters depict this behavior qualitatively (see [24], Fig. S3). An increase in the interface capacitance would move Z_1 lower and increase the impedance. An increase in interfacial resistance would move P_1 lower with a higher time constant. Impedimetric responses presented in Figs. 4(a) and 4(b) were monitored for two different DNA lengths (24 and 48 bp) (see [24], Table S-I). The Bode response with only buffer was recorded and used as a baseline. Strand D1 immobilization revealed a net increase in the interfacial resistance (parallel shift in P_1). Upon complementary (D2) strand addition, P_1 was seen to move further in with the clear formation of Z_1, indicating relaxation of the adsorbed DNA film illustrated in Fig. 4(a). The reason we term it relaxation is because the rolloff in frequency does not follow the 20-dB/decade drop as would be expected of a constant capacitance. This indicates that relaxation is frequency dependent. The dc operating point was adjusted to maintain a constant output current via CG feedback. The bandwidth of the TIA set a limit on the high-frequency response, which explains the rapid rolloff close to 1 MHz. Shorter 24-bp DNA strands (C1) upon hybridization, on the contrary, showed an outward movement of P_1 [Fig. 4(b)], possibly indicating a decreased resistance with a very weak formation of Z_1, which is consistent with recent evidence [4]. A plausible explanation is that the counterion cloud around the DNA molecule has not yet undergone complete relaxation and can still respond to the applied frequency [50]. This affects the resistance and capacitance of DNA as the counterion cloud effectively shields the signal. An interesting point is that the appreciable shift in Z_1 for the larger D1 and D2 strands occurs only when the oligonucleotides undergo hybridization (see Fig. 5). This seems to imply that the frequency-dependent nature of the relaxation is affected by the physical structure of the molecule since dsDNA is much more rigid than ssDNA [18,35] and leads to a different relaxation mechanism.

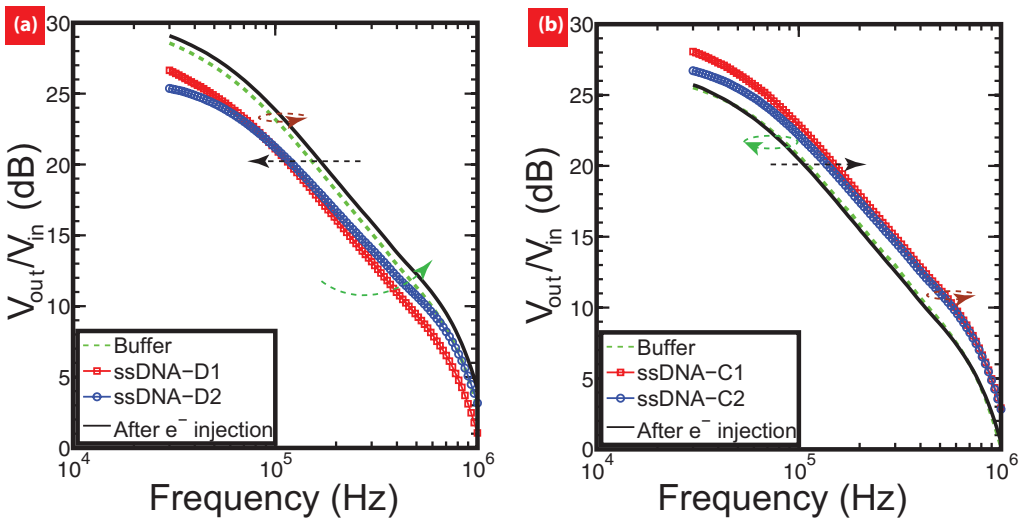

FIG. 5. (Color online) (a) DNA strands D1 and D2 are added to the chip in sequence and the frequency response before and after hybridization is monitored. A clear relaxation Z_1 is observed after hybridization, indicating that dispersion mechanisms are possibly tied to the structure and stiffness of the DNA strand. Charge injection is shown to refresh the surface with a recovery of impedance. (b) Step (a) repeated for strands C1 and C2, showing the molecular weight dependence on the formation of Z_1, which is very weak. The initial shift in P_1 is attributed to shift in resistance due to an inefficient relaxation at extremely small molecular length scales.

Upon programming (electron injection) the FG, we observed a recovery of P_1 and Z_1 to their respective initial points of pure buffer. This is in agreement with the quasistatic analysis where a recovery of ψ_O was observed. Impedimetric spectroscopy using FETs at a constant operating point is immune to any drift in solution pH and reliably probes the dielectric properties and local molecular structure. The impedance technique could potentially be used to ascertain local interactions between DNA and proteins where charge and capacitance can be concomitantly detected and serve as a versatile test bench in biophysical applications.

V. CONCLUSION

We present sensing and dynamic manipulation of surface-immobilized DNA using the CνMOS. Quasistatic IV and impedance spectroscopy measurements were performed. The measured ψ_O during DNA immobilization and hybridization was found to be electric-field dependent. A positive electric field enhanced the hybridization and immobilization signal, while a negative electric field reduced it. In addition, dual-gate control and charge programmed onto the FG affected the sensitivity by inducing different field conditions in the SG oxide. Manipulation of the oligonucleotides was realized via nonvolatile charge injection, which set a defined repulsive or attractive field between the FG and solution. The ionic cloud and associated descreening around DNA is believed to be responsible for this effect as it can be perturbed [32,51] via the field effect. This was further corroborated by modeling the DNA membrane using modified screening and partition energy formulations. The modified permittivity due to the partition energy difference, which could arise due to either orientation or ion-specific exclusion effects, was found to play a key role. Furthermore $V_{\text{th\_CG}}$ and ψ_O were observed to recover after DNA desorption aided by the noncovalent nature of the binding. Impedimetric detection using a split-gate approach showed a clear shift in the frequency response upon DNA immobilization (pole) and subsequent hybridization (pole and zero). Two different lengths were tested (24 and 48 bp) and the results indicate that the impedance recovers upon charge injection, indicating surface recovery. The frequency response was also found to exhibit a molecular weight and structure dependence. Upon programming the FG with electrons, the interface impedance was observed to recover, indicating DNA desorption. This technique of combined detection and manipulation using chemoreceptive metal-oxide-semiconductor compatible charge sensors can potentially help realize electrically addressable sensor arrays, refreshable biosensor interfaces, and dynamic reconfiguration of protein complexes.

ACKNOWLEDGMENTS

This work was supported by NSF MRSEC Grant No. DMR 0520404 through Cornell Center for Materials Research Interdisciplinary Research Group. We would like to thank Professor Lois Pollack for thoughtful discussions and insights provided during the course of DNA experimentation and validation. We acknowledge the Cornell, Nano Biotechnology Center, and Cornell Nano-Scale Facility for allowing us to use their facilities. K.J would like to thank Yang Liu of Stanford University for useful discussions on the Donnan potential. K.J would like to thank Mark R Hartman of Professor Dan Luo's group at Cornell and Lihua Wang and Lee Li of Professor Lois Pollack's group for assistance in DNA preparation.

[1] L. Bandiera *et al.*, Biosens. Bioelectron. **22**, 2108 (2007).
[2] M. Barbaro, A. Bonfiglio, and L. Raffo, IEEE Trans. Electron Devices **53**, 158 (2006).
[3] J. Fritz *et al.*, Proc. Natl. Acad. Sci. USA **99**, 14142 (2002).
[4] R. GhoshMoulick *et al.*, Phys. Status. Solidi A **206**, 417 (2009).
[5] B. C. Jacquot *et al.*, Biosens. Bioelectron. **23**, 1503 (2008).
[6] E. Katz and I. Willner, Electroanalysis **15**, 913 (2003).
[7] F. Uslu *et al.*, Biosens. Bioelectron. **19**, 1723 (2004).
[8] A. Star *et al.*, Proc. Natl. Acad. Sci. USA **103**, 921 (2006).
[9] G. Zheng *et al.*, Nat. Biotechnol. **23**, 1294 (2005).
[10] K. Jayant, T. Porri, J. W. Erickson, and E. C. Kan, in *Proceedings of the 15th International Conference on Solid-State Sensors, Actuators and Microsystems, Denver, 2009* (IEEE, Piscataway, NJ, 2009), p. 1814.
[11] O. Knopfmacher *et al.*, Nano Lett. **10**, 2268 (2010).
[12] C. Baozhen, A. Parashar, and S. Pandey, IEEE Sens. J. **11**, 2906 (2011).
[13] P. Bergveld, Sens. Actuat. B **88**, 1 (2003).
[14] N. Y. M. Shen *et al.*, IEEE Trans. Electron Devices **50**, 2171 (2003).
[15] E. Stern *et al.*, Nature (London) **445**, 519 (2007).
[16] A. Gao *et al.*, Nano Lett. **11**, 3974 (2011).
[17] Y. L. Bunimovich *et al.*, J. Am. Chem. Soc. **128**, 16323 (2006).
[18] U. Rant *et al.*, Biophys. J. **85**, 3858 (2003).
[19] M. Erdmann *et al.*, Nat. Nano **5**, 154 (2010).
[20] I. Y. Wong and N. A. Melosh, Nano Lett. **9**, 3521 (2009).
[21] F. Fixe *et al.*, Biosens. Bioelectron. **19**, 1591 (2004).
[22] B. Reddy, Jr. *et al.*, Anal. Chem. **83**, 888 (2011).
[23] K. Jayant, K. Auluck, M. Funke, S. Anwar, J. B. Phelps, P. H. Gordon, S. R. Rajwade, and E. C. Kan, Phys. Rev. E **88**, 012801 (2013).
[24] See Supplemental Material at http://link.aps.org/supplemental/10.1103/PhysRevE.88.012802 for additional details of the instrumentation setup, control experiments for DNA hybridization, and simulation of the DNA-transistor impedance model. Tables outlining the oligonucleotides used and equation set describing the working of the CνMOS transistor are also included.
[25] A. Vainrub and B. M. Pettitt, Phys. Rev. E **66**, 041905 (2002).
[26] A. B. Kharitonov *et al.*, J. Phys. Chem. B **105**, 4205 (2001).
[27] A. H. Talasaz *et al.*, Proc. Natl. Acad. Sci. USA **103**, 14773 (2006).
[28] D. Landheer *et al.*, J. Appl. Phys. **98**, 044701 (2005).
[29] D. Landheer *et al.*, IEEE Sens. J. **7**, 1233 (2007).

[30] R. B. M. Schasfoort *et al.*, Anal. Chim. Acta **238**, 323 (1990).
[31] J. Kruise *et al.*, Sens. Actuat. B **6**, 101 (1992).
[32] W. R. McKinnon, D. Landheer, and G. Aers, J. Appl. Phys. **104**, 124701 (2008).
[33] G. Shalev, Y. Rosenwaks, and I. Levy, Biosens. Bioelectron. **31**, 510 (2012).
[34] Y. Liu and R. W. Dutton, J. Appl. Phys. **106**, 014701 (2009).
[35] W. Kaiser and U. Rant, J. Am. Chem. Soc. **132**, 7935 (2010).
[36] I. Y. Wong and N. A. Melosh, Biophys. J. **98**, 2954 (2010).
[37] A. B. Kharitonov *et al.*, J. Electroanal. Chem. **487**, 133 (2000).
[38] A. B. Kharitonov *et al.*, Sens. Actuat. B **70**, 222 (2000).
[39] S. Ingebrandt *et al.*, Biosens. Bioelectron. **22**, 2834 (2007).
[40] T. M. Squires, R. J. Messinger, and S. R. Manalis, Nat. Biotechnol. **26**, 417 (2008).
[41] X. T. Vu *et al.*, Sens. Actuat. B **144**, 354 (2010).
[42] A. Poghossian *et al.*, Sens. Actuat. B **111-112**, 470 (2005).
[43] T. Windbacher, V. Sverdlov, and S. Selberherr, in *Proceedings of 13th International Workshop on Computational Electronics, IWCE 2009, Beijing, 2009* (IEEE, Piscataway, NJ, 2009), p. 1.
[44] C. Heitzinger *et al.*, J. Comput. Theor. Nanosci. **7**, 2574 (2010).
[45] J. Israelachvilli, *Intermolecular & Surface Forces* (Academic, London, 1992).
[46] P. Fromherz, Phys. Status Solidi A **209**, 1157 (2012).
[47] M. Denhoff and D. Landheer, ECS Trans. **35**, 17 (2011).
[48] Z. Jiang and D. Stein, Langmuir **26**, 8161 (2010).
[49] M. M. G. Antonisse *et al.*, Anal. Chem. **72**, 343 (1999).
[50] S. Takashima, Biopolymers **5**, 899 (1967).
[51] Y. Liu *et al.*, Appl. Phys. Lett. **97**, 143109 (2010).